Nitric Acid−Water Complexes: Theoretical Calculations and Comparison to Experiment†

Patrick R. McCurdy, Wayne P. Hess, and Sotiris S. Xantheas*

William R. Wiley Environmental Molecular Sciences Laboratory, Pacific Northwest National Laboratory, P.O. Box 999, MS K8-91, Richland, Washington 99352

Received: January 28, 2002; In Final Form: March 21, 2002

The formation of $HNO_3 \cdot (H_2O)_n$ complexes is studied both theoretically and experimentally. First principles electronic structure calculations were used to produce minimum structures and harmonic vibrational frequencies of $HNO_3 \cdot (H_2O)_n$ and $DNO_3 \cdot (H_2O)_n$ complexes ($n = 0-4$). They also provide insight into the ionization of HNO_3 in water, predicting that ionization in isolated clusters occurs for $n = 4$ or larger. Vibrational absorption spectra of matrix isolated nitric acid/water complexes were obtained using an FTIR spectrometer-based instrument. By incrementally increasing the amount of H_2O in the matrix, we have been able to study nitric acid/water complexes and the ionization of HNO_3. New spectral assignments, the first ones for the $n = 2$ and 3 complexes, are suggested on the basis of the results of the electronic structure calculations.

I. Introduction

Proton transfer is an important aspect of acid−base equilibria, electrochemistry, and various processes in biological systems such as enzymatic catalysis, photosynthesis, and transport across membranes. It has been established that proton transfer does not occur for 1:1 complexes of even strong acids and water (e.g., $HCl \cdot H_2O$[1] and $HNO_3 \cdot H_2O$[2]). Instead, acidic proton transfer is a process involving several solvent water molecules acting together to stabilize the proton-anion pair. Water molecules can stabilize proton transfer between other acceptor donor systems. For example, the nitric acid-ammonia complex has been shown to be molecular when isolated in a matrix or in the gas-phase, but in an aqueous environment, the $NH_4^+ - NO_3^-$ pair becomes the more stable form.[3−5] Extensive theoretical work on processes related to proton transfer in polar solvents has been reported.[4−11] Despite this effort, the mechanism of solvation and ionization of acids remains unclear due to the complexity of solution phase reactions, and proton tunneling effects.

Nitric acid and its hydrates play an important role in atmospheric chemistry.[12] In the stratosphere, nitric acid hydrates are the primary components of the type I polar stratospheric clouds—a key player in the seasonal depletion of polar ozone. Alternatively, the relative stability of HNO_3 allows transport to the troposphere where it gives rise to acid rain. The macroscopic properties of the binary nitric acid − water system are an essential element of a multicomponent thermodynamic model that describes atmospheric processes. To this end, extensive studies of the binary system's properties such as thin film crystallization kinetics,[13,14] vapor pressure measurements,[15] nucleation,[16] phase transitions,[17] and its role in heterogeneous atmospheric reactions[18] have been reported. Furthermore, the formation, stability[19] and reactions[20] of aqueous clusters of nitric acid were studied in molecular beam experiemnts that provided molecular level information. Ritzhaupt and Devlin[2] have previously studied $HNO_3 \cdot H_2O$ complexes in Ar matrixes using FTIR spectroscopy. They concluded that at low concentrations of water in the matrix (<3%) $HNO_3 \cdot H_2O$ exists primarily as a molecular complex, and above this concentration the solvated ion pair becomes important. A significant splitting in the asymmetric stretch ($\Delta\nu_3$) of the NO_3^- ion was noted that varied with the degree of solvation. In a later study of solid H_2O-HNO_3 mixtures,[21] the same authors suggested as many as three water molecules may be required to ionize the HNO_3 molecule. However, no definitive conclusions were drawn, and no direct evidence for the existence of higher order molecular species other than the 1:1 complex was presented. Barnes et al.[3] have also previously studied $HNO_3 \cdot H_2O$ complexes in Ar matrixes using FTIR spectroscopy. Their study focused on the $H-ONO_2$ stretching region of the complex in 1:1:200 HNO_3:H_2O:Ar matrixes.

In the present study we investigate the formation of $HNO_3 \cdot (H_2O)_n$ complexes from first principles electronic structure methods and compare our findings to new and previously reported experimental results. The calculations yielded optimized ground-state structures and harmonic vibrational frequencies for the $HNO_3 \cdot (H_2O)_n$ ($n = 0-5$) clusters and their DNO_3 analogues. We also present new FTIR data and discuss spectral assignments in light of the new theoretical results. The calculated results aid in the interpretation of the matrix isolated FTIR spectra, indicating that dissociation occurs for cluster sizes greater than $n = 4$.

II. Theoretical and Experimental Methods

First principles electronic structure calculations were performed to determine structures and vibrational frequencies for the $HNO_3(H_2O)_n$, $n = 0-4$ clusters. We obtained optimal structures and computed harmonic vibrational frequencies for these clusters and their deuterated DNO_3 analogues at the second-order perturbation level[22] of theory (MP2) using the augmented correlation consistent polarized valence double-ζ (aug-cc-pVDZ) orbital basis set.[23] This level of theory has been chosen as a compromise between accuracy and feasibility of the calculations especially for the larger clusters as it has been previously shown to produce reliable results for the structures and frequencies of hydrogen bonded neutral[24] clusters as well as clusters of water with positive[25] and negative ions.[26] Additional calculations at the same level of theory were performed to obtain structures and frequencies for H_2O, D_2O,

† Part of the special issue "G. Wilse Robinson Festschrift".

10.1021/jp020257e CCC: $22.00
Published on Web 05/14/2002

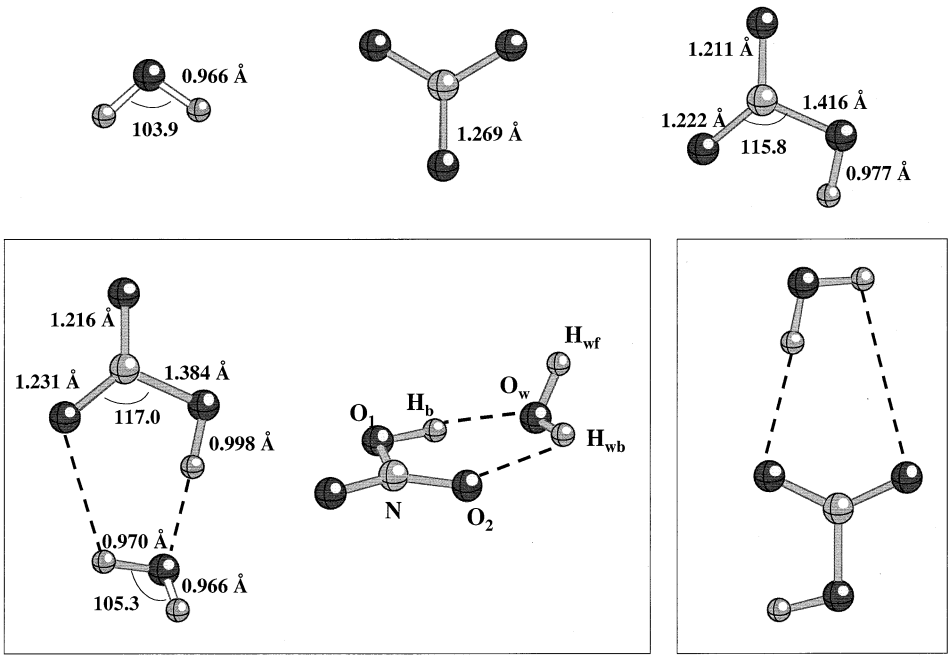

Figure 1. Optimal geometries of H_2O, NO_3^-, HNO_3 and $HNO_3(H_2O)$. Bond distances are in Å, and bond angles in degrees.

and $(H_2O)_2$ and $(D_2O)_2$ complexes. The calculations were performed using the Gaussian-94[27] and NWChem[28] suites of electronic structure codes. The calculations do not explicitly account for the effect of the matrix (Ar).

Experiments were conducted using a matrix-isolation FTIR apparatus described previously.[29] Argon solutions of HNO_3 and H_2O or their deuterated analogues (DNO_3 and D_2O) were co-deposited from separate nozzles onto KBr substrates cooled to 12 K by a closed-cycle helium cryostat. For annealed samples, FTIR spectra were taken at 12 K after annealing for 5 min at the indicated temperature. Thin films were vapor deposited to a thickness of approximately 40 μm over a period of approximately 2 h. HNO_3 vapor was collected from a 1:2 (by volume) mixture of fuming HNO_3 (99.5) and H_2SO_4 (96%) designed to reduce the minor NO_2 vapor component. DNO_3 was produced by reacting D_2SO_4 (98%) with KNO_3 (99%). Delivery lines were passivated overnight with D_2O before delivery of DNO_3 to minimize hydrogen isotope exchange. Thin film growth was monitored by recording the interference fringes of a reflected helium−neon laser beam aligned at a near-normal incidence to the substrate. FTIR spectra of condensed samples were collected for 256 scans at a resolution of 1 cm^{-1}.

III. Results

a. Minimum Energy Structures. The optimal geometries of H_2O, NO_3^-, HNO_3 and the $HNO_3(H_2O)$ cluster at the MP2/aug-cc-pVDZ level of theory are shown in Figure 1. The NO_3^- anion has D_{3h} symmetry, whereas the symmetry of HNO_3 is C_s. The lowest energy conformation of the $HNO_3(H_2O)$ cluster corresponds to a cyclic, homodromic[30] arrangement in which the water molecule acts as a proton acceptor from nitric acid's hydrogen atom, in agreement with previous calculations[31] and the structure obtained from the fitting of the microwave spectra.[32] The system forms a quasi-planar, six-membered ring with the free atom of the water molecule lying above the molecular plane. The path corresponding to the wagging motion of this atom above and below the plane passes via a planar transition state with a barrier[31] of 83 cm^{-1}.

The strength of the $HNO_3{\cdot}(H_2O)$ hydrogen bond with respect to the separated fragments is 10.3 kcal/mol (8.1 kcal/mol when harmonic zero-point corrections are included). This value is about twice that of the hydrogen bond in the water dimer.[33,34] The slight deviation from linearity is similar to that in the water dimer (the $O_w-H_b-O_1$ angle is 174.7° vs 171.3° in the water dimer[34]), while the separation between the two heavy atoms participating in the hydrogen bond (O_w and O_1 in Figure 1) is 2.708 Å, about 0.208 Å shorter than the corresponding one in the water dimer at the same level of theory (MP2/aug-cc-pVDZ).[34] The strong hydrogen bond results in an elongation of the hydrogen bonded OH bond length by 0.021 Å with respect to the isolated nitric acid fragment, a value that is three times larger than the corresponding bond lengthening of 0.007 Å in the water dimer. This, in turn, is expected to induce a large red shift in the corresponding stretching frequency,[35] as a consequence of Badger's rule.[36] Indeed, the harmonic frequency of the hydrogen bonded O_1-H_b stretch in $HNO_3{\cdot}(H_2O)$ is 3284 cm^{-1}, a decrease of 420 cm^{-1} from the calculated harmonic frequency of 3704 cm^{-1} for the nitric acid monomer.

TABLE 1: Calculated Structural Parameters for the Nitric Acid−Water Cluster and Comparison with Previous Calculations and Experimental Results[a]

	theoretical		experimentally fitted[32]	
parameter	ref 31	this work	fully distorted monomers	"preferred" structure
$R(H_b-O_w)$, Å	1.707	1.713	1.812	1.779
$\alpha(O_1-H_b-O_w)$, deg	176.4	174.7	170.4	174.5
$\beta(H_b-O_w-H_{wb})$, deg	101.3	97.2	93.4	92
$\gamma[H_{wf}-(O_w-H_b-O_1)]$, deg	49.9	42.8	30.3	30
$R(H_{wb}-O_2)$, Å	2.49	2.39	2.27	2.30
$q(O_2-H_{wb}-O_w)$, deg	108	113.0	118.9	119.3

[a] The labeling of the atoms used to define the structural parameters is shown in Figure 1.

Our value for the binding energy is slightly larger than the 9.5 kcal/mol value reported by Tao et al.[31] Our computed MP2/aug-cc-pVDZ structural parameters for the 1:1 complex together with the theoretical result of Tao et al.[31] and the parameters obtained from the fitting of the microwave spectra[32] are listed in Table 1. Two sets of data are shown for the experimentally fitted structure. The first one uses fully distorted monomers (using the theoretically predicted changes in the fragment

TABLE 2: Calculated Harmonic Frequencies (cm^{-1}) for the Various Complexes. Symmetric and antisymmetric OH stretches are indicated by "ss" and "as", respectively

species	mode	HNO_3 [DNO_3]	$HNO_3 \cdot H_2O$ [$DNO_3 \cdot H_2O$]	$HNO_3 \cdot (H_2O)_2$ [$DNO_3 \cdot (H_2O)_2$]	$HNO_3 \cdot (H_2O)_3$ [$DNO_3 \cdot (H_2O)_3$]	$(HNO_3)_2$ [$(DNO_3)_2$]	H_2O [D_2O]	$(H_2O)_2$ [$(D_{2O})_2$]
HNO_3 [DNO_3]	ν_1 OH str	3704 [2696]	3284 [2397]	3050 [2235]	2887 [2121]	3465 [2525] as 3410 [2490] ss		
	ν_2 asym NO_2 str	1861 [1848]	1831 [1807]	1809 [1786]	1809 [1776]	1816 [1791] ss 1809 [1790] as		
	ν_3 NOH bend	1349 [1040]	1504 [1140]	1507 [1140]	1556 [1179]	1468 [1115] ss 1449 [1104] as		
	ν_4 sym NO_2 str	1321 [1321]	1335 [1334]	1348 [1348]	1354 [1354]	1363 [1364] as 1312 [1312] ss		
	ν_5 N−O str	878 [878]	940 [938]	974 [972]	987 [985]	959 [954] as 956 [955] ss		
	ν_6 NO_2 scissors	653 [649]	687 [683]	698 [694]	699 [694]	702 [670] as 688 [684] ss		
	ν_7 ONO_2 in plane	578 [541]	637 [607]	640 [608]	663 [638]	623 [592] as 620 [587] ss		
	ν_8 ONO_2 out of plane	763 [762]	775 [776]	778 [780]	787 [787]	790 [773] as 772 [771] ss		
	ν_9 NO−H torsion	487 [360]	869 [642]	981 [724]	999 [720]	745 [551] as 689 [498] ss		
H_2O [D_2O]	ν_1 OH str		3906 [3906]as 3770 [3769]ss	3903 [3903] as 3876 [3876] ss 3756 [3756] as[a] 3516 [3512] ss[a]			3938 [2885] as 3804 [2743] ss	3925 [2876] as 3904 [2855] ss 3796 [2738] as[a] 3704 [2678] ss[a]
H_2O [D_2O]	ν_2 HOH bend		1615 [1613]	1654 [1651] 1618 [1617]			1622 [1187]	1643 [1200] 1624 [1190]

[a] Participating in H-bond.

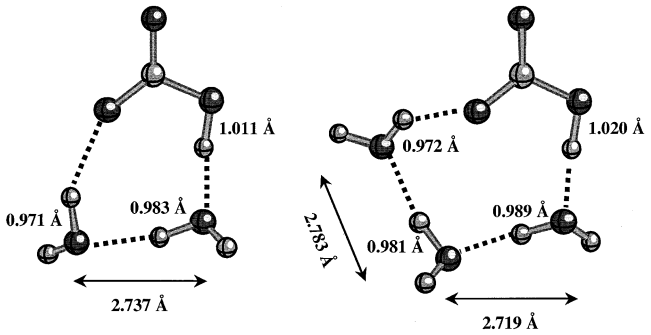

Figure 2. Optimal geometries of $HNO_3(H_2O)_n$, $n = 2, 3$. The values of the hydrogen bonded OH stretches and the interoxygen distances between water molecules (Å) are shown.

geometries) as well as the average of the intermolecular structural parameters obtained from fits using the undistorted and fully distorted monomer geometries, denoted as "preferred" structure in Table 1. Our results are closer to the experimentally obtained structural parameters than the previous calculation[31] and the remaining differences can be attributed both to the basis set and to the effect of large-amplitude motion that is contained in the fitting of the experimental data. A previously unexplored arrangement, in which the water molecule acts primarily as a proton donor to nitric acid (cf. Figure 1), corresponds to a local minimum lying 7.3 kcal/mol above the global minimum (6.3 kcal/mol with zero-point energy corrections). This is a consequence of the fact that HNO_3 in the gas phase is a stronger acid than water. The harmonic frequencies of the $HNO_3 \cdot (H_2O)_n$ and $DNO_3 \cdot (H_2O)_n$ up to $n = 3$, as well as for the $(H_2O)_2$ and $(D_2O)_2$ dimers are given in Table 2.

The structural motif of homodromic rings that incorporate water molecules continues for the larger clusters $HNO_3 \cdot (H_2O)_n$, $n = 2, 3$. The optimal structures for these clusters are shown in Figure 2. The corresponding binding energies are 20.6 (16.2) kcal/mol and 30.4 (23.7) kcal/mol for the $n = 2$ and 3 clusters, respectively, where numbers in parentheses include zero-point energy corrections. The strong cooperative effect that drives the formation of these rings[37] is evident from the large elongation of nitric acid's hydrogen bonded OH. It amounts to 1.011 Å for $n = 2$ and 1.020 Å for $n = 3$ (cf. Figure 2), resulting in lengthenings of 0.034 and 0.043 Å and corresponding red shifts of 654 and 816 cm^{-1} in the OH stretching frequencies with respect to isolated HNO_3. Our FTIR data (*vide infra*) provide evidence to support this prediction as we have tentatively identified nitric acid's O−H stretch bands corresponding to clusters with 1, 2, and 3 water molecules. The O−H stretch band of the $n = 3$ cluster is weak and highly broadened. As regards the hydrogen bonding between water molecules, the fragment containing two water molecules of the $n = 2$ cluster corresponds to a "compact" water dimer having an O−O separation of 2.737 Å, viz. 0.179 Å shorter than the corresponding one in the gas-phase water dimer. This trend continues for the larger $n = 3$ cluster where the O−O separation is now 0.08 Å shorter than the corresponding one in the cyclic water trimer.[38] Our calculations further indicate that the $HNO_3(H_2O)_3$ cluster does not support a stable "ion pair" configuration.

The first stable ion-pair configuration is encountered as a local minimum for $n = 4$. Indeed for this cluster we locate two stable structures, a global $HNO_3 \cdot (H_2O)_4$ minimum and a local $H_3O^+(H_2O)_3NO_3^-$ minimum lying just 0.4 kcal/mol above the global minimum. These are shown in Figure 3. Zero-point energy corrections increase the separation between the two minima to 1.5 kcal/mol. The corresponding binding energies of the two minima with respect to the (HNO_3 + 4 H_2O) asymptote are 40.5 (31.4) kcal/mol and 40.1 (29.9) kcal/mol, respectively.

b. FTIR Spectra. The spectra of HNO_3:H_2O:Ar and DNO_3:H_2O:Ar matrixes were obtained at various dilution factors and compared with the measured spectra of equivalent HNO_3:Ar and H_2O:Ar mixtures. Spectra of HNO_3:H_2O:Ar matrixes show several distinct features that do not correlate to either HNO_3 or H_2O species and therefore are assigned to nitric acid−water complexes. Table 3 includes various experimental band assignments for these complexes from the present work and that of previous studies.[3,39]

TABLE 3: Measured Frequencies (cm^{-1}) for the Various Complexes in Ar Matrix

mode	HNO_3	$HNO_3{\cdot}H_2O$	$HNO_3{\cdot}(H_2O)_2$	$(HNO_3)_2$	DNO_3	$DNO_3{\cdot}H_2O$	$DNO_3{\cdot}(H_2O)_2$	$(DNO_3)_2$
ν_1 OH str of HNO_3	3522[a]	3025[a]	2600	3235[a]	2601[b]	2292	2017	2415
$\nu_2 + \nu_4$		3126[a]		3216[a]				2395
$\nu_2 + \nu_3$		2980[a]						
$2\nu_4$		2784[a]				2161		
ν_2 NO_2 asym str	1699[a]	1694[a]	1670	1680[a]	1678[b]	1644	1637	1638
ν_3 NOH bend	1304[a]	1412[a]		1380[a]	1013[b]	1096	1115	1070
ν_4 NO_2 sym str	1321	1308[a]		1315[a]	1310[b]			1322
ν_5 N−O str	897[a]	931[a]	950	938[a]	894[b]	930	948	936
			960	944			959	
ν_6 NO_2 scissors	656[a]				650[b]			
ν_7 ONO_2 in plane	588[a]				548[b]			
ν_8 ONO_2 out of plane	764[a]	770[a]			763[b]	776	780	770
ν_9 HON torsion	451[a]			693[a]				

[a] Reference 3. [b] Reference 39.

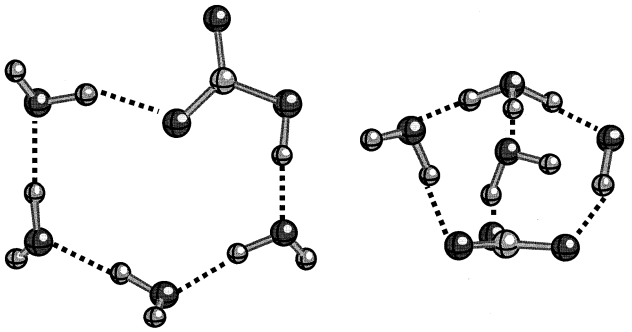

Figure 3. Global $HNO_3(H_2O)_4$ and local $H_3O^+(H_2O)_3NO_3^-$ minima for the $n = 4$ cluster.

Figure 4 displays the spectra from DNO_3:H_2O:Ar matrixes between 1900 and 2650 cm^{-1}, a region relatively free of interference due to overlapping bands. The O−D stretching bands associated with $DNO_3(H_2O)_n$ clusters up to $n = 3$ are apparent as the water concentration is increased (cf. Figure 4). The strongest feature in the low water concentration matrix (1:5:200) is the O−D stretch of the DNO_3 monomer at 2601 cm^{-1} seen in Figure 4a. In the higher water concentration spectrum, two strong bands centered at 2292 and 2161 cm^{-1} are evident, as is a strong broad feature near 2017 cm^{-1}. These bands are shifted from the DNO_3 monomer O−D stretch frequency by −309, −440, and −586 cm^{-1}, respectively, which compares very well with the calculated harmonic shifts of −299, −461, and −575 cm^{-1} for the $DNO_3(H_2O)_n$ clusters, $n = 1$, 2, 3. The integrated band intensity of the isolated DNO_3 O−D stretch feature decreases sharply in the high water concentration spectrum indicating that nearly all DNO_3 forms a complex with water. The integrated band intensities of the features at 2292 and 2161 cm^{-1} also decrease with increasing water concentration, while the broad feature at 2017 cm^{-1} increases.

Figure 4b displays matrix spectra of HNO_3 and $HNO_3(H_2O)_n$ clusters in the H−ONO_2 stretch region between 2400 and 3850 cm^{-1}. Unlike the DNO_3 spectra of Figure 4a, the H−ONO_2 stretch region suffers from interference due to overlapping bands of water and larger $(H_2O)_n$ clusters. The O−H stretching bands associated with $HNO_3(H_2O)_n$ clusters up to $n = 3$ can nonetheless be identified. The strongest feature in the 1:5:200 matrix is again the (offscale) O−H stretch fundamental of the nitric acid monomer. In the region where the two OH stretches of the $HNO_3{\cdot}(H_2O)$ and $HNO_3{\cdot}(H_2O)_2$ complexes are expected, we observe four bands. These four bands, centered at 2784, 2981, 3024, and 3131 cm^{-1}, were assigned by Barnes et al.[3] as arising from the $HNO_3(H_2O)$ complex. Three of the bands were attributed to "Fermi resonances" with overtones and combination bands: $2\nu_4$ at 2784 cm^{-1}; $(\nu_2 + \nu_3)$ at 2981 cm^{-1}; and $(\nu_2 + \nu_4)$ at 3130 cm^{-1}. The remaining band at 3024 cm^{-1} was assigned[3] to the ν_1 O−H stretch of the $HNO_3(H_2O)$ complex.

TABLE 4: Calculated and Measured Frequency Shifts (cm^{-1}) for Deuterated Nitric Acid/Water Complexes[a]

n	$\Delta\nu_1$ measd	$\Delta\omega_1$ calcd	$\Delta\nu_5$ measd	$\Delta\omega_5$ calcd	$\Delta\nu_3$ measd	$\Delta\omega_3$ calcd
			$DNO_3(H_2O)_n$			
1	−309	−299	43	60	83	100
2	−440	−462	61	90		100
3	−575	−586	72	107	101	139
			$HNO_3(H_2O)_n$			
1	−496	−420	34	62	107	155
2	−734	−654	54	94	109	158
3	−907	−817	65	109	131	207

[a] See Table 3 for the assignment of the modes.

In our spectra an additional broad feature centered at 2613 cm^{-1} is observed. If we assume that the band centered at 3024 cm^{-1} is assigned correctly as the $HNO_3{\cdot}(H_2O)$ O−H stretch, then the calculated frequency shifts indicate that the absorptions centered at 2784 and 2613 cm^{-1} should be assigned as O−H stretch modes for the $HNO_3{\cdot}(H_2O)_2$ and $HNO_3{\cdot}(H_2O)_3$ complexes, respectively. Table 4 presents a comparison between the calculated and experimentally determined frequency shifts for the ν_1, ν_3, and ν_5, bands. The broad absorption feature and sharp bands observed above 3150 cm^{-1} are attributable to water clusters. Although we expect the integrated band intensity of the isolated HNO_3 O−H stretch feature to be small and that nearly all HNO_3 forms complexes with water molecules, spectral interference currently prevents confirmation of this assertion.

Figure 5a shows the FTIR spectra of the DO−NO_2 stretch region for DNO_3:H_2O:Ar matrixes as a function of increasing H_2O ratio. The prominent peak at 887 cm^{-1} in the upper trace is assigned to ν_5, the DO−NO_2 stretch of the monomer, while the peak at 1013 cm^{-1} is due to the D−O−NO_2 bending mode. As expected, these peaks decrease in intensity as the concentration of H_2O in the matrix is increased, and the spectra displays features associated with hydrated DNO_3 species. The top trace of Figure 5a shows a series of peaks between 920 and 950 cm^{-1}. The sharp band centered at 930 cm^{-1} is present only in mixtures containing both DNO_3 and H_2O and is assigned to the $DNO_3{\cdot}H_2O$ complex. Two additional broad weak bands centered at 948 and 960 cm^{-1} are apparent. We assign these two peaks to the $DNO_3{\cdot}(H_2O)_2$ and $DNO_3{\cdot}(H_2O)_3$ complexes. The relative integrated absorption of the 948 and 960 cm^{-1} bands is greatest in the 1:20:200 sample.

Very little isolated DNO_3 is detected in the 1:20:200 sample, as shown by the loss of the DO−NO_2 band at 894 cm^{-1}, and

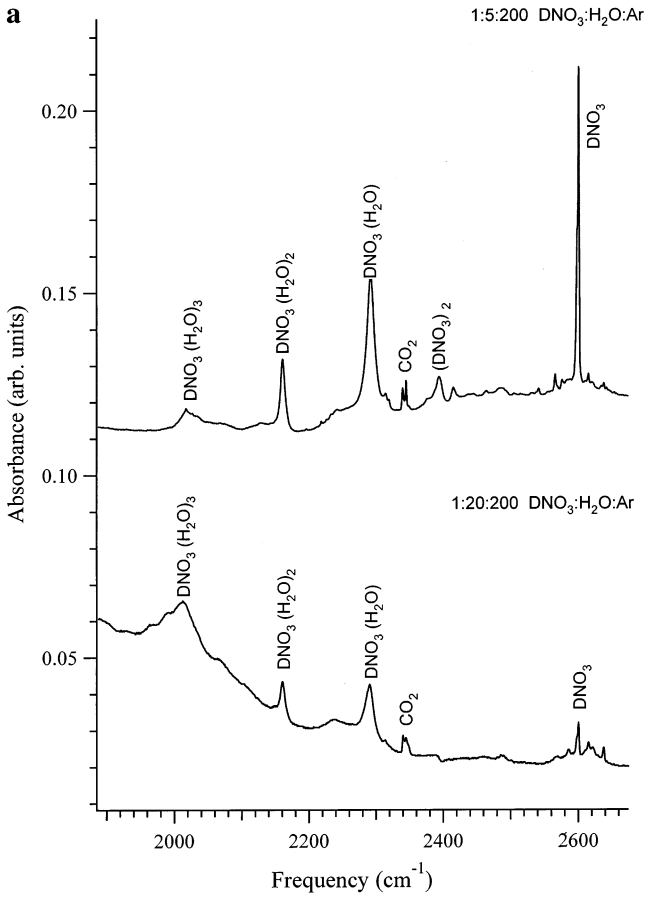

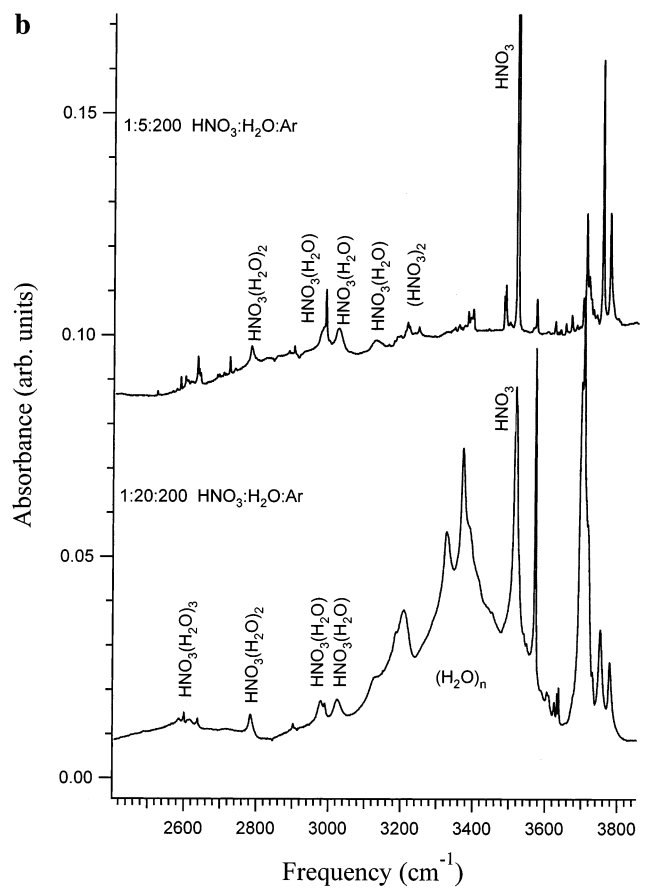

Figure 4. FTIR absorption spectra of the O−D and O−H stretch bands for (a) DNO_3:H_2O:Ar matrixes and (b) HNO_3:H_2O:Ar matrixes at 1:5:200 (upper trace) and 1:20:200 (lower trace) gas precursor ratios.

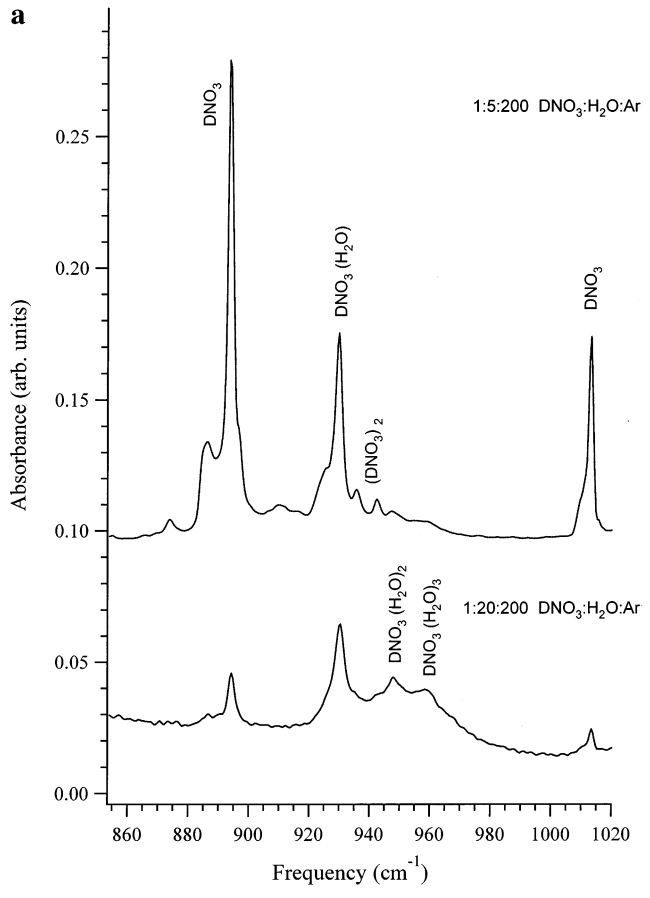

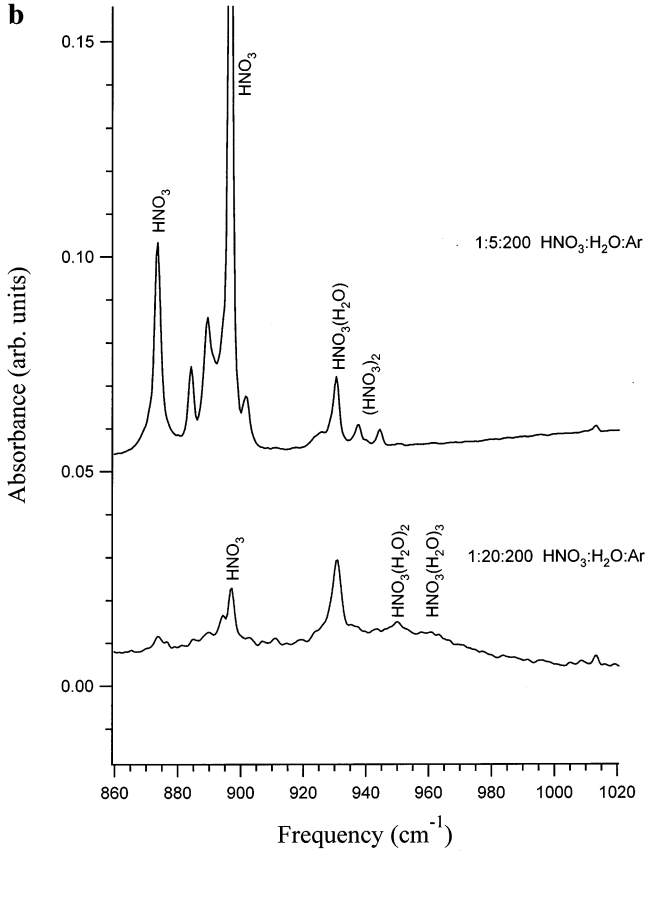

Figure 5. FTIR absorption spectra of the O−N stretch bands for (a) DNO_3:H_2O:Ar matrixes and (b) HNO_3:H_2O:Ar matrixes at 1:5:200 (upper trace) and 1:20:200 (lower trace) gas precursor ratios.

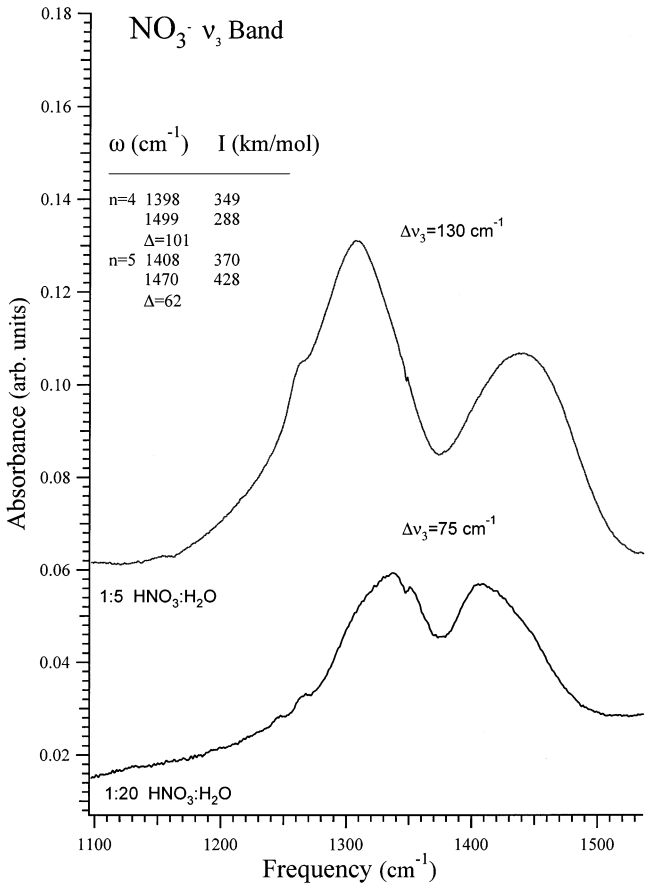

Figure 6. FTIR spectra of a 1:5 HNO_3:H_2O matrix (top), and a 1:20 HNO_3:H_2O matrix. The argon component was removed from the initially prepared matrix by annealing at 40 K for 10 min.

the greatly diminished D−O−NO_2 bend at 1013 cm^{-1}. Figure 5b displays the analogous spectra and assignments for HNO_3·$(H_2O)_n$ complexes. Band assignments are presented in Table 3 and the comparison between calculated and observed frequency shifts is shown in Table 4. The peaks at 939 and 943 cm^{-1} are also observed when no water is present in the matrix. The predicted band center for the DNO_3 dimer is 955 cm^{-1} and we assign these bands to the DO−NO_2 stretch of $(DNO_3)_2$. At the highest water concentration, the 939 and 943 cm^{-1} bands can no longer be distinguished in the spectrum indicating that DNO_3 dimer species are hydrated.

Interestingly, at this high water concentration one would expect an abundance of species of higher order than the DNO_3·$(H_2O)_3$ complex to be formed. However, the spectrum shows no unambiguous features attributable to higher order DNO_3·$(H_2O)_n$ ($n > 3$) species. The most likely cause for the lack of discernible higher order hydrates is the dissociation of DNO_3 to a partially hydrated ion pair. The strongest NO_3^- modes observed in the 1:20:200 spectrum are the degenerate ν_3 vibrations between 1250 and 1500 cm^{-1}. As concluded by Ritzhaupt and Devlin,[21] these bands are assigned to the asymmetric stretch of the NO_3^- anion that is hydrogen bonded to a hydronium ion. When the NO_3^- is in contact with a counterion, this degeneracy is lifted and a splitting into the ν_{3a} and ν_{3b} bands occurs. As the contact ion pair is increasingly solvated, the splitting of the NO_3^- ν_3 vibrations decreases. These bands have also been recently observed[40] during FTIR spectroscopic studies of water uptake on α-Al_2O_3 particles previously reacted with HNO_3. Figure 6 shows the spectra of 1:5:200 versus 1:20:200 (HNO_3:H_2O:Ar) samples annealed at 40 K for 10 min. The annealing process evaporates argon from the matrix and thus increases the percent water (and nitric acid) concentration of the matrix. The relative degree of anion solvation is apparent, indicated by the splitting of the ν_{3a} and ν_{3b} bands, $\Delta\nu_3$, which decreases from ∼130 to ∼75 cm^{-1}. For comparison, the calculated splitting and band intensities of the NO_3^- bands for the ion-pair complexes with 4 and 5 water molecules, is also displayed in Figure 6. We note that the calculated band splittings for the incremental solvation of the $H_3O^+(H_2O)_3NO_3^-$ ion-pair complex reproduce the trend observed experimentally quite accurately.

IV. Discussion

The frequency shifts calculated for the D−ONO_2·$(H_2O)_n$ clusters ($n = 1-3$) show quantitative agreement with the measured FTIR data. In particular, the O−D stretch spectral region displays bands separated by frequency intervals rather accurately predicted by our calculations. Qualitative agreement is also found for the O−H spectral region of the HNO_3·$(H_2O)_n$ system and the N−OD stretch and N−O-D bend spectral regions of the DNO_3·$(H_2O)_n$ system. On the strength of the correspondence between the calculated and experimental results, we may tentatively assign the measured bands for the nitric acid−water clusters up to $n = 3$ (cf. Table 3).

Given the fact that the computed frequencies are obtained at the harmonic approximation, we choose to compare the calculated frequency shifts, $\Delta\omega$, rather than their absolute values, to the experimentally obtained frequency shifts, $\Delta\nu$. This correspondence has been previously successfully used to assign IR bands for negative ion−water clusters.[26] The difference between the harmonic and observed frequencies is strongly mode dependent with the OH stretching modes usually displaying the greatest discrepancy due to the large (>150 cm^{-1}) anharmonicities of these high-frequency modes. For instance, the calculated harmonic frequency of 3704 cm^{-1} for the H−ONO_2 stretch mode is significantly larger than the observed gas-phase frequency of 3551 cm^{-1} and the Ar matrix isolated value of 3522 cm^{-1}. Modes with smaller anharmonicities can show much better correspondence between calculated and measured frequencies, such as the calculated frequency of 653 cm^{-1} for the ν_6 NO_2 scissors mode, which is very close to the measured gas-phase value of 650 cm^{-1}. When using frequency shifts to guide spectral assignment, we assume that, for each particular mode, the anharmonicities are similar even for clusters of different sizes and therefore the frequency shifts, to first order, are independent of error due to the harmonic approximation.

We regard our band assignments as tentative due to some ambiguities apparent in the experimental results and discrepancies with the interpretations of results published by other researchers. The most likely cause for the discrepancies is the effect of the argon matrix environment. The formation of clusters within the argon matrix cannot be controlled ideally by simply changing the deposition conditions. We have no control over, or indeed much knowledge of, the distribution of various clusters within the matrix. The cluster distribution depends on the backing pressure and concentration of precursor gases, the deposition rate, the temperature of the substrate and the anneal history of the sample. Although all these factors are controllable, there is no clear extrapolation from any particular set of growth conditions to the actual cluster distribution. Furthermore, any particular cluster could occupy a variety of matrix environments or configurations. The exact effects of varying the deposition conditions and anneal history are not known. Since the cluster distribution is unknown, we can only expect integrated band intensities to reflect differences in growth conditions in a qualitative fashion.

If a set of absorption bands is identified as arising from a particular species (e.g., $DNO_3 \cdot H_2O$) then it is normally assumed that the relative integrated intensity of the associated bands will be constant regardless of the species concentration. Conversely, if two absorption features display constant relative integrated band intensities, regardless of matrix concentration, then they are likely derived from the same species. This reasoning previously led Barnes et al.[3] to conclude that the four bands centered at 2784, 2981, 3024, and 3131 cm^{-1}, observed in HNO_3:H_2O:Ar matrixes, are assigned to the $HNO_3 \cdot H_2O$ complex. Since we also observe that the relative band intensities of these features are nearly constant as the water concentration is varied, we are tempted to make the same conclusion. However, on the strength of the results of the ab initio calculations, we tentatively assign the band centered at 2784 cm^{-1} to the $HNO_3 \cdot (H_2O)_2$ complex and the band centered at 2613 cm^{-1} to the $HNO_3 \cdot (H_2O)_3$ complex. This latter band displays the expected increase in integrated intensity with water concentration. This assignment is further strengthened by the qualitative agreement of the ab initio results with the observed spectral features for several vibrational modes of the $n = 2$ and 3 clusters.

In our experiments Ar acts as a solvent, providing some degree of stabilization to ionic species. Even though the calculations indicate that dissociation into ion pairs requires at least four water molecules to stabilize the isolated clusters, it may require less than four water molecules to produce a matrix isolated ion pair if the solid argon solution provides sufficient stabilization. Matrix-isolated species (solute) can be regarded as molecules in a solution of matrix (solvent) molecules. Theoretical models used to account for the solvent effects on vibrational spectra interpret frequency shifts in terms of specific solute/solvent interactions (electrostatic) superimposed on nonspecific (inductive and dispersive) contributions. It is known that molecular vibrational frequencies are shifted in an argon matrix environment because of this effect.[41,42]

The O−H stretch of HNO_3 in the gas-phase is observed at 3551 cm^{-1},[43] while in an Ar matrix this stretch is red-shifted by 29 cm^{-1} to 3522 cm^{-1}. To illustrate the effect of the argon matrix on molecules and their complexes, let us consider the vibrational spectrum of methanol and its dimer. In the gas phase, the OH stretch of the proton donating molecule of the dimer is red-shifted by 107 cm^{-1} from the monomer value,[44] while in an Ar matrix the OH stretch is red-shifted by 135 cm^{-1} from the monomer.[42] This indicates that H-bonded complexes in matrix environments can experience significantly large frequency shifts with respect to their monomers than their gas-phase counterparts (see for example ref 45)

Figure 4a shows two peaks (2292 and 2161 cm^{-1}) in the region where the OD stretch of the $DNO_3 \cdot H_2O$ complex is expected. The ratio of their integrated intensities as a function of H_2O concentration is nearly constant, suggesting they could be derived from the same species. While it is clear that the band centered at 2292 cm^{-1} is due to the O−D stretch of the $DNO_3 \cdot H_2O$ complex, the second band is shifted by −440 cm^{-1} from O−D stretch of the isolated monomer, which compares remarkably well (−462 cm^{-1}) to the calculated shift in the $DNO_3 \cdot (H_2O)_2$ complex. The assignment of this band to the $DNO_3 \cdot (H_2O)_2$ complex is also supported by the similar behavior of the band assigned to the $DNO_3(H_2O)_2$ complex for the DO−NO_2 stretch, which is shifted by 60 cm^{-1}.

The $HNO_3 \cdot H_2O$ complex actually shows four separate peaks separated by more than 300 cm^{-1}in the OH stretch region. Barnes et al.[3] have previously assigned three of these peaks to Fermi resonance interactions giving rise to overtones from other vibrational modes of the $HNO_3 \cdot H_2O$ complex. The fact that only two analogous peaks are observed in the corresponding portion of the FTIR spectrum for the DNO_3/H_2O/Ar matrix support this explanation for at least two of the peaks seen in the HNO_3/H_2O/Ar spectrum. Still, no combination of frequencies for the $DNO_3 \cdot H_2O$ complex match the observed frequency and hence we assign the band centered at 2162 cm^{-1} to the $DNO_3(H_2O)_2$ complex. Figure 4a also shows a broad peak at ∼2015 cm^{-1}. This peak is not observed in very low water concentration spectra (not shown here) but is clearly observed in the 1:5:200 spectrum. The integrated absorption intensity of the band centered at ∼2015 cm^{-1} increases with water concentration and the band broadens further. We assign this band to the $DNO_3 \cdot (H_2O)_3$ complex.

V. Conclusions

We present the results of ab initio calculations for the structures and vibrational spectra of the $HNO_3 \cdot (H_2O)_n$ ($n = 0-4$) complexes and their deuterated analogues in an effort to provide insight into the ionization of HNO_3 in an aqueous environment and aid in the assignment of the experimental FTIR spectra obtained in a matrix environment. The calculations predict the appearance of ion-pair configurations in the gas phase for $n = 4$. These results were used to interpret matrix isolation spectra of $HNO_3 \cdot (H_2O)_n$ complexers. While HNO_3:H_2O:Ar matrixes have been studied previously, we present the first spectroscopic evidence for the existence of the $HNO_3 \cdot (H_2O)_2$ and $HNO_3 \cdot (H_2O)_3$ complexes in these environments. Interestingly, spectra for larger clusters were not observed. The experimental assignments are in agreement with the results of our cluster calculations that indicate that four water molecules are needed to stabilize ion pair configurations. This finding is consistent with the one of Ritzhaupt and Devlin[21] in their previous study of H_2O/HNO_3 solid mixtures where they mainly observed molecular species in low ratio mixtures and concluded "perhaps as many as three waters of hydration are required to stabilize the ionized form." Our results for the $n = 1$ cluster are largely consistent with Barnes et al.[3] although we tentatively reassign one band to the $n = 2$ complex rather than a combination band of the $n = 1$ complex on the basis of the cluster calculations presented in this study.

Acknowledgment. This work was performed in the William R. Wiley Environmental Molecular Sciences Laboratory (EMSL) under the auspices of the Division of Chemical Sciences, Office of Basic Energy Sciences, U.S. Department of Energy under Contract DE-AC06-76RLO 1830 with Battelle Memorial Institute, which operates the Pacific Northwest National Laboratory. The EMSL is a national user facility funded by the Office of Biological and Environmental Research in the U.S. Department of Energy. Computer resources were provided by the Division of Chemical Sciences, U.S. Department of Energy.

References and Notes

(1) Ault, B. S.; Pimentel, G. C. *J. Phys. Chem.* **1973**, *77*, 57 .
(2) Ritzhaupt, G.; Devlin, J. P. *J. Phys. Chem.* **1977**, *81*, 521.
(3) Barnes, A. J.; Lasson, E.; Nielsen, C. J. *J. Mol. Struct.* **1994**, *322*, 165.
(4) Tao, F.-M. *J. Chem. Phys.* **1998**, *108*, 193.
(5) Nguyen, M.-T.; Jamka, A. J.; Cazar, R. A.; Tao, F.-M. *J. Chem. Phys.* **1997**, *106*, 8710.
(6) Smith, B. J.; Branson, K.; Schüürmann, G. *Chem. Phys. Lett.* **2001**, *342*, 402.
(7) Staib, A.; Borgis, D.; Hynes, J. T. *J. Chem. Phys.* **1995**, *102*, 2487.

(8) Ando, K.; Hynes, J. T. *J. Phys. Chem. B* **1997**, *101*, 10464.
(9) Ando, K.; Hynes, J. T. *J. Phys. Chem. A* **1999**, *103*, 10398.
(10) Wesolowski, T.; Muller, R. P.; Warshel, A. *J. Phys. Chem*. **1996**, *100*, 15444.
(11) Pérez, P.; Contreras, R.; Aizman, A. *J. Phys. Chem*. **1996**, *100*, 19326.
(12) Hamill, P.; Toon, O. B. *Phys. Today* **1991**, Dec, 34.
(13) Disselkamp, R. S.; Anthony, S. E.; Prenni, A. J.; Onasch, T. B.; Tolbert, M. A. *J. Phys. Chem.* **1996**, *100*, 9127.
(14) Tisdale, R. T.; Middlebrook, A. M.; Prenni, A. J.; Tolbert, M. A. *J. Phys. Chem. A* **1997**, *101*, 2112.
(15) Zhang, R.; Wooldridge, P. J.; Molina, M. J. *J. Phys. Chem.* **1993**, *97*, 8541.
(16) Mirabel, P.; Clavelin, J. L. *J. Chem. Phys.* **1978**, *68*, 5020.
(17) H.-Y. Chang, A.; T. Koop. Molina, L. T.; Molina, M. J. *J. Phys. Chem. A* **1999**, *103*, 2673.
(18) For a recent review see Zondlo, M. A.; Barone, S. B.; Tolbert, M. A. *J. Phys. Chem. A* **1998**, *102*, 5735.
(19) Kay, B. D.; Hermann, V.; Castleman, A. W., Jr. *Chem. Phys. Lett.* **1981**, *80*, 469.
(20) Lee, N.; Keesee, R. G.; Castleman, A. W., Jr. *J. Chem. Phys.* **1980**, *72*, 1089. Zhang, X.; Mereand, E. L.; Castleman, A. W., Jr. *J. Phys. Chem.* **1994**, *98*, 3554.
(21) Ritzhaupt, G.; Devlin, J. P. *J. Phys. Chem*. **1991**, *95*, 90.
(22) Møller, C.; Plesset, M. S. *Phys. Rev.* **1934**, *46*, 618.
(23) Dunning, T. H., Jr. *J. Chem. Phys.* **1989**, *90*, 1007. Kendall, R. A.; Dunning, T. H., Jr.; Harrison, R. J. *J. Chem. Phys.* **1992**, *96*, 6796.
(24) Xantheas, S. S.; Dunning, T. H., Jr. *J. Chem. Phys.* **1993**, *99*, 8774. Xantheas, S. S. *J. Chem. Phys.* **1994**, *100*, 7523. Dang, L. X.; Feller, D. *J. Phys. Chem. B* **2000**, *104*, 4403.
(25) Feller, D.; Glendening, E. D.; Kendall, R. A.; Peterson, K. A. *J. Chem. Phys.* **1994**, *100*, 4981. Feller, D.; Glendening, E. D.; Woon, D. E.; Feyereisen, M. W. *J. Chem. Phys.* **1995**, *103*, 3526. Glendening, E. D.; Feller, D. *J. Phys. Chem.* **1995**, *99*, 3060. Glendening, E. D.; Feller, D. *J. Chem. Phys.* **1996**, *100*, 4790. Wasserman, E.; Rustad, J. R.; Xantheas, S. S. *J. Chem. Phys.* **1997**, *106*, 9769. Feller, D.; Glendening, E. D.; de Jong, W. A. *J. Chem. Phys.* **1999**, *110*, 1475.
(26) Xantheas, S. S.; Dunning, T. H., Jr. *J. Phys. Chem.* **1992**, *96*, 7505. Xantheas, S. S.; Dunning, T. H., Jr. *J. Phys. Chem.* **1994**, *98*, 13489. Xantheas, S. S. *J. Am. Chem. Soc.* **1995**, *117*, 10373. Xantheas, S. S. *J. Phys. Chem.* **1996**, *100*, 9703. Cabarcos, O. M.; Weinheimer, C. J.; Lisy, J. M. Xantheas, S. S. *J. Chem. Phys.* **1999**, *110*, 5. Ayotte, P.; Nielsen, S. B.; Weddle, G. H.; Johnson, M. A. Xantheas, S. S. *J. Phys. Chem. A* **1999**, *103*, 10665.
(27) Frisch, M. J.; Trucks, G. W.; Schlegel, H. B.; Gill, P. M. W.; Johnson, B. G.; Robb, M. A.; Cheeseman, J. R.; Keith, T.; Petersson, G. A.; Montgomery, J. A.; Raghavachari, K.; Al-Laham, M. A.; Zakrzewski, V. G.; Ortiz, J. V.; Foresman, J. B.; Cioslowski, J.; Stefanov, B. B.; Nanayakkara, A.; Challacombe, M.; Peng, C. Y.; Ayala, P. Y.; Chen, W.; Wong, M. W.; Andres, J. L.; Replogle, E. S.; Gomperts, R.; Martin, R. L.; Fox, D. J.; Binkley, J. S.; Defrees, D. J.; Baker, J.; Stewart, J. P.; Head-Gordon, M.; Gonzalez, C.; Pople, J. A. *Gaussian 94*, revision E.2; Gaussian, Inc.: Pittsburgh, PA, 1995.
(28) J. Anchell, et al. NWChem, Version 3.3.1, Pacific Northwest National Laboratory, Richland, WA, 1999. See *http://www.emsl.pnl.gov* for more information.
(29) Rowland, B.; Hess, W. P. *J. Phys. Chem. A* **1997**, *101*, 8049.
(30) Tzeli, D.; Mavridis, A. Xantheas, S. S. *Chem. Phys. Lett.* **2001**, *340*, 538.
(31) Tao, F.-M.; Higgins, K.; Klemperer, W.; Nelson, D. D. *Geophys. Res. Lett.* **1996**, *23*, 1797.
(32) Canagaratna, M.; Phillips, J. A.; Ott, M. E.; Leopold, K. R. *J. Phys. Chem. A* **1998**, *102*, 1489.
(33) Feyereisen, M. W.; Feller, D.; Dixon, D. A. *J. Phys. Chem.* **1996**, *100*, 2993. Halkier, A.; Koch, H.; Jorgensen, P.; Christiansen, O.; Nielsen, I. M. B.; Helgaker, T. *Theor. Chem. Acc.* **1997**, *97*, 150.
(34) Xantheas, S. S. *J. Chem. Phys.* **1996**, *104*, 8821.
(35) Xantheas, S. S.; Dunning, T. H., Jr. In *Advances in Molecular Vibrations and Collision Dynamics*; Bacic, Z., Bowman, J. M., Eds.; JAI Press, London, 1998; Vol. 3, pp 281.
(36) Badger, R. M. *J. Chem. Phys.* **1934**, *2*, 128; **1935**, *3*, 710.
(37) Xantheas, S. S. *Chem. Phys.* **2000**, *258*, 225.
(38) Xantheas, S. S.; Dunning, T. H., Jr. *J. Chem. Phys.* **1993**, *98*, 8037.
(39) Mielke, Z.; Schriver-Mazzuoli, L.; Schriver, A. *J. Phys. Chem. A* **1997**, *101*, 4560.
(40) Goodman, A. L.; Bernard, E. T.; Grassian, V. H. *J. Phys. Chem. A* **2001**, *105*, 6443.
(41) Jagannathan, S.; Cooper, J. R.; Wilkins, C. L. *Appl. Spectrosc*. **1989**, *43*, 781.
(42) Behrens-Griesenbach, A.; Luck, W. A. P.; Schrems, O. *J. Chem. Soc., Faraday Trans. 2* **1984**, *80*, 579.
(43) McGraw, G. E.; Bernitt, D. L.; Hisatsune, I. C. *J. Chem. Phys*. **1965**, *42*, 237.
(44) Huisken, F.; Kulcke, A. *J. Phys. Chem*. **1991**, *95*, 3924.
(45) Andrews, L.; Wang, X. *J. Phys. Chem. A* **2001**, *105*, 7541.